

Resource Allocation and Dithering of Bayesian Parameter Estimation Using Mixed-Resolution Data

Itai E. Berman, *Student Member, IEEE* and Tirza Routtenberg, *Senior Member, IEEE*

Abstract—Quantization of signals is an integral part of modern signal processing applications, such as sensing, communication, and inference. While signal quantization provides many physical advantages, it usually degrades the subsequent estimation performance that is based on quantized data. In order to maintain physical constraints and simultaneously bring substantial performance gain, in this work we consider systems with mixed-resolution, 1-bit quantized and continuous-valued, data. First, we describe the linear minimum mean-squared error (LMMSE) estimator and its associated mean-squared error (MSE) for the general mixed-resolution model. However, the MSE of the LMMSE requires matrix inversion in which the number of measurements defines the matrix dimensions and thus, is not a tractable tool for optimization and system design. Therefore, we present the linear Gaussian orthonormal (LGO) measurement model and derive a closed-form analytic expression for the MSE of the LMMSE estimator under this model. In addition, we present two common special cases of the LGO model: 1) scalar parameter estimation and 2) channel estimation in mixed-ADC multiple-input multiple-output (MIMO) communication systems. We then solve the resource allocation optimization problem of the LGO model with the proposed tractable form of the MSE as an objective function and under a power constraint using a one-dimensional search. Moreover, we present the concept of dithering for mixed-resolution models and optimize the dithering noise as part of the resource allocation optimization problem for two dithering schemes: 1) adding noise only to the quantized measurements and 2) adding noise to both measurement types. Finally, we present simulations that demonstrate the advantages of using mixed-resolution measurements and the possible improvement introduced with dithering and resource allocation.

Index Terms—Massive MIMO, resource allocation, mixed-ADC, linear minimum mean-squared error, dithering

I. INTRODUCTION

Traditional statistical signal processing (SSP) techniques were developed for high-resolution sensors, under the unrealistic assumption of infinite precision sampling, or “analog” data, that can neglect the quantization effect. High-resolution sensors result in high performance in various SSP tasks, such as parameter estimation. In modern signal processing, signal quantization plays an important role with various applications, including wireless sensor networks (WSNs) [1]–[5], direction of arrival estimation [6], target tracking [7]–[9], multiple-input multiple-output (MIMO) communications [10]–[17], cognitive radio [18], and array processing [19]. For example, in communication systems there is usually a need

for cheaper, less power-hungry analog-to-digital converters (ADCs) while maintaining accurate channel estimation [13]. The widespread use of signal quantization is due to its many advantages, which include reduction of hardware complexity, power consumption, communication bandwidth, sensor cost, and sensor’s physical dimensions, as well as enabling high-rate sampling [20], [21]. Despite all its practical advantages, quantization results in low-resolution signals, which degrades the performance of subsequent parameter estimation that is based on the quantized data. Moreover, signal quantization introduces nonlinear effects into the system, which poses new challenges for parameter estimation that relies on these signals, such as non-convex optimizations [22], [23].

The nonlinear problem of parameter estimation based on low-precision samples, especially from 1-bit (signed) measurements has been discussed widely in the literature (see, e.g. [23]–[27]). For instance, in [1], [2], [28] the maximum-likelihood (ML) estimator and the corresponding Cramér-Rao bounds (CRBs) for quantized samples are presented. However, the ML is usually intractable, and, thus, various suboptimal, low-complexity methods have been developed in the literature [14], [19], [24], [29]. In [30] the problem of parameter estimation of a random parameter using 1-bit dithered measurements is studied, deriving lower bounds on the mean-squared error (MSE) using the Bayesian CRB and designing dither strategies. Studies on channel estimation in massive MIMO systems with 1-bit ADCs show acceptable performance in channel capacity and the achievable rate due to the use of a large number of antennas compared to that of analog ADCs [10], [31], [32]. In all these methods the use of quantized data results in a degradation of the estimation performance compared with the analog-data based methods.

In addition to purely-quantized or purely-analog data, a few works have been using schemes with multiple quantization resolution data [4], [13], [33]. For example, the ML and CRB for non-Bayesian estimation with partially quantized observations is considered in [33]. For the Bayesian case, the minimum MSE (MMSE) estimation of a uniformly distributed parameter, based on both quantized and unquantized observations, has been suggested in [4] and linear MMSE (LMMSE) in specific applications is discussed in [11], [12], [15]. However, while there are various estimation algorithms based on quantized signals (see above), there has been less emphasis on the analysis and design of mixed-resolution architectures. Considerable improvements could be obtained by optimization of estimation schemes relying on both quantized and continuous-valued data with respect to their parameters, performance, and complexity. This optimization is crucial in order to cope with the limited

This work is partially supported by the ISRAEL SCIENCE FOUNDATION (ISF), grant No. 1173/16.

I. Berman and T. Routtenberg are with the School of Electrical and Computer Engineering Ben-Gurion University of the Negev Beer-Sheva 84105, Israel, e-mail: itaieliy@post.bgu.ac.il, tirzar@bgu.ac.il.

resources for data processing, storage, and communication in real-world applications. However, incorporating quantized data results in non-trivial operations, creating a need for new tools. A main example is that, in contrast with continuous value data, using dithering, i.e. adding noise to a signal prior to its quantization, improves the estimation performance based on this signal [22], [34], [35]. However, while there are various estimation algorithms based on quantized signals, there has been less emphasis on the analysis and design of mixed-resolution architectures.

In this work, we consider Bayesian parameter estimation in systems with mixed-resolution, analog and 1-bit quantized, measurements. We develop the LMMSE estimator and its associated MSE for the considered model. We present the linear Gaussian orthonormal (LGO) measurement model, which is shown to generalize common schemes, including: 1) scalar parameter estimation and 2) channel estimation in mixed-ADC massive MIMO communication systems. A closed-form analytic expression of the MSE of the LMMSE estimator is derived under the LGO measurement model. The resource allocation problem is formalized under the LGO model with the tractable expression of the MSE as the objective function and under power constraints, and solved using a one-dimensional search over value pairs. The concept of dithering, the addition of noise to the measurements before quantization, is presented for the mixed-resolution scheme and the resource allocation problem is solved while also optimizing the dithering noise. Finally, simulations for the LGO model have been conducted and have shown the advantages of mixed-resolution estimation compared with purely-quantized or purely-analog settings, for the scalar case and for channel estimation in massive MIMO. In addition, the possible improvement from dithering can be seen even when adding the noise to both the analog and quantized measurements.

The remainder of the paper is organized as follows: Section II presents the general mixed-resolution measurement model and the resource allocation problem which is shown to be computationally tedious. In Section III, the LGO measurement model is presented and the resource allocation problem is solved for the LGO model, including dithering design. In Section IV, special cases of the LGO model are discussed. Simulations of the resource allocation method are given in Section V. Finally, our conclusions can be found in Section VI.

Notation: We use boldface lowercase letters to denote vectors and boldface capital letters for matrices. The identity matrix of size $M \times M$ is denoted by \mathbf{I}_M and vector of ones of length N is denoted by $\mathbf{1}_N$. The symbols $(\cdot)^*$, $(\cdot)^T$, and $(\cdot)^H$ represent the conjugate, transpose, and conjugate transpose operators, respectively. The symbol \otimes is the Kronecker product. We use $\text{trace}(\mathbf{A})$ to denote the trace of the matrix \mathbf{A} , and $\text{diag}(\mathbf{A})$ to denote a diagonal matrix containing only the diagonal elements of \mathbf{A} . The $\arcsin(\cdot)$ function, when applied to a vector or matrix, is applied elementwisely. The distribution of a circularly symmetric complex Gaussian random vector with mean $\boldsymbol{\mu}$ and covariance matrix $\boldsymbol{\Sigma}$ is denoted by $\mathcal{CN}(\boldsymbol{\mu}, \boldsymbol{\Sigma})$ and from here on noted as complex Gaussian. We denote the covariance matrix of a vector \mathbf{a} as

$\mathbf{C}_a = \mathbb{E}[\mathbf{a}\mathbf{a}^H]$ and correlation between vectors \mathbf{a} and \mathbf{b} as $\mathbf{C}_{ab} = \mathbb{E}[\mathbf{a}\mathbf{b}^H]$. The set of non-negative integers is denoted by \mathbb{Z}_+ . The 1-bit element-wise quantization function is applied separately on the real, $\text{Re}(z)$, and imaginary, $\text{Im}(z)$, part of any complex number $z \in \mathbb{C}$, and is defined as

$$\mathcal{Q}(z) = \frac{1}{\sqrt{2}} \left[\begin{array}{l} 1, \text{Re}(z) \geq 0 \\ -1, \text{Re}(z) < 0 \end{array} + j \begin{array}{l} 1, \text{Im}(z) \geq 0 \\ -1, \text{Im}(z) < 0 \end{array} \right]. \quad (1)$$

II. SYSTEM MODEL

In this section we present the system model and introduce the problem of parameter estimation using mixed-resolution measurements. In Subsection II-A the measurement model is presented and in Subsection II-B, the LMMSE estimator and its associated MSE are derived for the discussed model. Finally, in Subsection II-C we present the resource allocation optimization problem and discuss the difficulties of solving the problem.

A. General Mixed-Resolution Measurement Model

We consider the problem of estimating a random parameter vector based on mixed-resolution data. In particular, we assume a parameter vector, $\boldsymbol{\theta} \in \mathbb{C}^M$, with a zero-mean complex Gaussian distribution, $\boldsymbol{\theta} \sim \mathcal{CN}(\mathbf{0}, \boldsymbol{\Sigma}_\theta)$, where $\boldsymbol{\Sigma}_\theta$ is a known positive definite covariance matrix. The goal is to estimate $\boldsymbol{\theta}$ from a linear measurement model having both analog, high-resolution measurements:

$$\mathbf{x}_a = \mathbf{H}\boldsymbol{\theta} + \mathbf{w}_a, \quad (2)$$

and quantized, low-resolution measurements:

$$\mathbf{x}_q = \mathcal{Q}(\mathbf{G}\boldsymbol{\theta} + \mathbf{w}_q), \quad (3)$$

where the quantization operator, $\mathcal{Q}(\cdot)$, is defined in (1). The matrices $\mathbf{H} \in \mathbb{C}^{N_a \times M}$ and $\mathbf{G} \in \mathbb{C}^{N_q \times M}$ are known, with N_a and N_q being the number of analog and quantized measurements, respectively, and the added noise vectors, \mathbf{w}_a and \mathbf{w}_q , are independent, zero-mean, complex Gaussian noise, i.e. $\mathbf{w}_a \sim \mathcal{CN}(\mathbf{0}, \sigma_a^2 \mathbf{I}_{N_a})$ and $\mathbf{w}_q \sim \mathcal{CN}(\mathbf{0}, \sigma_q^2 \mathbf{I}_{N_q})$. It is also assumed that the noise vectors, \mathbf{w}_a and \mathbf{w}_q , and the unknown parameter vector, $\boldsymbol{\theta}$, are mutually independent. As a result, the analog measurements follow a complex Gaussian distribution, i.e. $\mathbf{x}_a \sim \mathcal{CN}(\mathbf{0}, \mathbf{C}_{x_a})$, with the covariance matrix

$$\mathbf{C}_{x_a} = \mathbf{H}\boldsymbol{\Sigma}_\theta\mathbf{H}^H + \sigma_a^2\mathbf{I}_{N_a}. \quad (4)$$

Similarly, the vector

$$\mathbf{y} \triangleq \mathbf{G}\boldsymbol{\theta} + \mathbf{w}_q \quad (5)$$

is a complex Gaussian vector, i.e. $\mathbf{y} \sim \mathcal{CN}(\mathbf{0}, \mathbf{C}_y)$, with the covariance matrix

$$\mathbf{C}_y = \mathbf{G}\boldsymbol{\Sigma}_\theta\mathbf{G}^H + \sigma_q^2\mathbf{I}_{N_q}. \quad (6)$$

In particular, (3) implies that $\mathbb{E}[\mathbf{x}_q] = \mathbf{0}$. However, the distribution of the quantized measurements \mathbf{x}_q in (3) does not have a closed-form expression for the general case. The goal

is to use mixed-resolution measurements, i.e. the augmented vector

$$\mathbf{x} \triangleq [\mathbf{x}_a^T \quad \mathbf{x}_q^T]^T, \quad (7)$$

to estimate $\boldsymbol{\theta}$ efficiently.

The considered model is fundamental in various signal processing applications with mixed-resolution data. An important case of this model, which is discussed in detail in Subsection IV-B, is channel estimation in massive MIMO communication systems. In this case, there are multiple users transmitting data to multiple antennas and the goal is to estimate the channel between users and each antenna, which is the unknown parameter vector $\boldsymbol{\theta}$ in this case. Due to system limitation, such as sensor power consumption, sensor cost, and channel capacity, part of the observed data is quantized at the antenna and sent the fusion center for estimation. This scenario, presented schematically in Fig. 1, can be interpreted as a joint distributed-centralized estimation setup in a MIMO communication system with partially-quantized measurements.

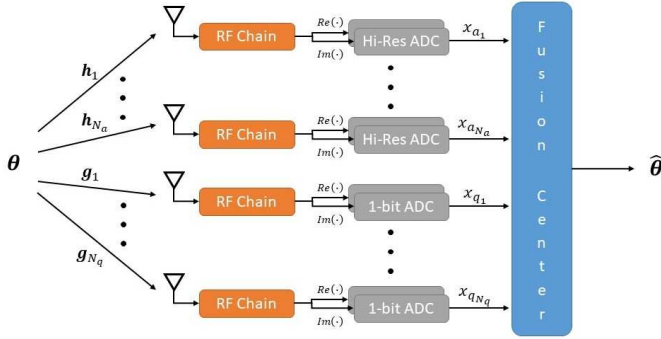


Fig. 1: Schematic system model of estimation with mixed-resolution data. A data vector, $\boldsymbol{\theta}$, is transmitted and received over a known channel and undergoes either a high- or 1-bit low-resolution quantization. The unknown data vector is then estimated from the mixed-resolution measurements in the fusion center.

B. LMMSE Estimation

The MMSE estimator of $\boldsymbol{\theta}$ based on the mixed-resolution data \mathbf{x} in (7) is given by the conditional expectation, $\hat{\boldsymbol{\theta}}^{\text{MMSE}} = \mathbb{E}[\boldsymbol{\theta}|\mathbf{x}]$. Derivation of the MMSE estimator requires an analytic form of the conditional probability distribution function, $f(\boldsymbol{\theta}|\mathbf{x})$, which does not have a closed-form expression in general in the presence of quantized measurements. Moreover, since the MMSE estimator is a function of both the analog (continuous valued) measurements and the quantized (discrete valued) measurements, then, even the numerical evaluation of $\hat{\boldsymbol{\theta}}^{\text{MMSE}}$ is intractable and requires multidimensional numerical integration. Therefore, usually the LMMSE estimator is used when quantized measurements are involved.

For the sake of simplicity of presentation, in the following, $\hat{\boldsymbol{\theta}}$ denotes the LMMSE estimator. For zero-mean measurements, as in our case, and under the assumption that \mathbf{C}_x is a non-singular matrix, the LMMSE estimator, based on both \mathbf{x}_a and

\mathbf{x}_q , is given by

$$\hat{\boldsymbol{\theta}} = \mathbf{C}_{\boldsymbol{\theta}\mathbf{x}} \mathbf{C}_x^{-1} \mathbf{x}, \quad (8)$$

and the associated MSE of the LMMSE estimator is

$$\begin{aligned} \text{MSE} &= \mathbb{E} \left[(\hat{\boldsymbol{\theta}} - \boldsymbol{\theta})^H (\hat{\boldsymbol{\theta}} - \boldsymbol{\theta}) \right] \\ &= \text{trace}(\boldsymbol{\Sigma}_{\boldsymbol{\theta}}) - \text{trace}(\mathbf{C}_{\boldsymbol{\theta}\mathbf{x}} \mathbf{C}_x^{-1} \mathbf{C}_{\boldsymbol{\theta}\mathbf{x}}^H). \end{aligned} \quad (9)$$

In Appendix A it is shown that the auto-covariance matrix of \mathbf{x} and the cross-covariance matrix of \mathbf{x} and $\boldsymbol{\theta}$ are block matrices given by

$$\mathbf{C}_x = \begin{bmatrix} \mathbf{H}\boldsymbol{\Sigma}_{\boldsymbol{\theta}}\mathbf{H}^H + \sigma_a^2 \mathbf{I}_{N_a} & \vdots \\ \left(\sqrt{\frac{2}{\pi}} \mathbf{H}\boldsymbol{\Sigma}_{\boldsymbol{\theta}}\mathbf{G}^H (\text{diag}(\mathbf{C}_y))^{-\frac{1}{2}} \right)^H & \vdots \\ \sqrt{\frac{2}{\pi}} \mathbf{H}\boldsymbol{\Sigma}_{\boldsymbol{\theta}}\mathbf{G}^H (\text{diag}(\mathbf{C}_y))^{-\frac{1}{2}} \\ \frac{2}{\pi} \left(\arcsin \left((\text{diag}(\mathbf{C}_y))^{-\frac{1}{2}} \text{Re}(\mathbf{C}_y) (\text{diag}(\mathbf{C}_y))^{-\frac{1}{2}} \right) \right. \\ \left. + j \arcsin \left((\text{diag}(\mathbf{C}_y))^{-\frac{1}{2}} \text{Im}(\mathbf{C}_y) (\text{diag}(\mathbf{C}_y))^{-\frac{1}{2}} \right) \right) \end{bmatrix} \quad (10)$$

and

$$\mathbf{C}_{\boldsymbol{\theta}\mathbf{x}} = \begin{bmatrix} \boldsymbol{\Sigma}_{\boldsymbol{\theta}}\mathbf{H}^H & \sqrt{\frac{2}{\pi}} \boldsymbol{\Sigma}_{\boldsymbol{\theta}}\mathbf{G}^H (\text{diag}(\mathbf{C}_y))^{-\frac{1}{2}} \end{bmatrix}, \quad (11)$$

respectively. By substituting (10) and (11) into (8) and (9) we obtain the LMMSE estimator and its associated MSE.

C. Optimization of MSE

The main goal in this paper is to find the optimal number of analog and quantized measurements, N_a^* and N_q^* , respectively, in the sense of minimum MSE of the associated LMMSE estimator, given in (9) under some physical constraints. That is, we aim to solve the following optimization problem,

$$\begin{aligned} \min_{N_a, N_q} \quad & \text{trace}(\boldsymbol{\Sigma}_{\boldsymbol{\theta}}) - \text{trace}(\mathbf{C}_{\boldsymbol{\theta}\mathbf{x}} \mathbf{C}_x^{-1} \mathbf{C}_{\boldsymbol{\theta}\mathbf{x}}^H) \\ \text{s.t.} \quad & \begin{cases} \mathbf{h}_1(N_a, N_q) \leq \mathbf{0} \\ \mathbf{h}_2(N_a, N_q) = \mathbf{0} \\ N_a, N_q \in \mathbb{Z}_+ \end{cases}, \end{aligned} \quad (12)$$

where $\mathbf{h}_1(N_a, N_q) \leq \mathbf{0}$ and $\mathbf{h}_2(N_a, N_q) = \mathbf{0}$ represent different inequality and equality constraints, respectively, which stem from physical system requirements. The optimization problem in (12) is an integer programming problem, which often leads to solutions of combinatorial nature that cannot be solved in a reasonable time, even for small datasets [36]. Moreover, since the decision variables N_a and N_q represent the dimensions of the matrices $\mathbf{C}_{\boldsymbol{\theta}\mathbf{x}}$ and \mathbf{C}_x in the objective function of (12), the problem cannot be solved by a simple relaxation that allows non-integer rational solutions. As a result, for each value pair of the decision variables, N_a and N_q , we need to calculate the inverse matrix, \mathbf{C}_x^{-1} , and perform matrix multiplication, giving a total computational complexity of $\mathcal{O}((N_a + N_q)^3 + 2M(N_a + N_q)^2)$, which increases as the number of measurements increases. This approach may be intractable and may hinder insights into the original problem.

III. OPTIMIZATION FOR THE ORTHONORMAL MEASUREMENT MODEL

In this section we present the LGO measurement model, optimize the resource allocation for this model, and propose the use of dithering. In Subsection III-A we present the LGO model and derive a tractable expression for the MSE under this model. In Subsection III-B we discuss some physical constraints common in real-world systems with mixed-resolution measurements and in Subsection III-C solve the resource allocation optimization problem under a constraint. In Subsection III-D the concept of dithering for the LGO model is discussed and two possible cases of the optimization problem are presented while allowing dithering.

A. Orthonormal Measurement Model

The LGO model is the model described in Subsection II.A, which also satisfies the following assumptions:

- A.1) The elements of $\boldsymbol{\theta}$ are uncorrelated with unit variance, i.e. $\boldsymbol{\Sigma}_{\boldsymbol{\theta}} = \mathbf{I}_M$.
- A.2) The matrix \mathbf{H} is a block matrix of size $N_a \times M$, where $N_a = Mn_a$:

$$\mathbf{H} = [\mathbf{H}_1 \quad \mathbf{H}_2 \quad \dots \quad \mathbf{H}_{n_a}]^T, \quad (13)$$

where each block satisfies

$$\mathbf{H}_i^H \mathbf{H}_j = \rho_a \mathbf{I}_M, \quad i = j \quad (14)$$

and $\rho_a > 0$. If $i \neq j$ then the product $\mathbf{H}_i^H \mathbf{H}_j$ can take arbitrary values.

- A.3) The matrix \mathbf{G} is a block matrix of size $N_q \times M$, where $N_q = Mn_q$, with equal blocks:

$$\mathbf{G} = \mathbf{1}_{n_q} \otimes \mathbf{G}_1, \quad (15)$$

where

$$\mathbf{G}_1^H \mathbf{G}_1 = \rho_q \mathbf{I}_M, \quad (16)$$

in which $\rho_q > 0$.

Theorem 1. *The LMMSE estimator for the mixed-resolution model, described in Subsection II-A and under Assumptions A.1-A.3, is*

$$\hat{\boldsymbol{\theta}} = \left[\left(\frac{1}{\rho_a n_a + \sigma_a^2} - \frac{2\rho_q n_q \sigma_a^2}{\pi(\rho_q + \sigma_q^2)(\alpha + \beta(n_a)\rho_q n_q)(\rho_a n_a + \sigma_a^2)^2} \right) \mathbf{H}^H \right. \\ \left. \sqrt{\frac{2}{\pi(\rho_q + \sigma_q^2)}} \frac{\sigma_a^2}{(\alpha + \beta(n_a)\rho_q n_q)(\rho_a n_a + \sigma_a^2)} \mathbf{G}^H \right] \mathbf{x} \quad (17)$$

and its associated MSE is

$$MSE = M - M \left(\frac{\rho_a n_a}{\rho_a n_a + \sigma_a^2} + \frac{2\rho_q n_q \sigma_a^4}{\pi(\rho_q + \sigma_q^2)(\alpha + \beta(n_a)\rho_q n_q)(\rho_a n_a + \sigma_a^2)^2} \right), \quad (18)$$

where

$$\alpha \triangleq 1 - \frac{2}{\pi} \arcsin \left(\frac{\rho_q}{\rho_q + \sigma_q^2} \right) = \frac{2}{\pi} \arccos \left(\frac{\rho_q}{\rho_q + \sigma_q^2} \right) \quad (19)$$

and

$$\beta(n_a) \triangleq \frac{2}{\pi} \arcsin \left(\frac{\rho_q}{\rho_q + \sigma_q^2} \right) \frac{1}{\rho_q} - \frac{2\rho_a n_a}{\pi(\rho_q + \sigma_q^2)(\rho_a n_a + \sigma_a^2)}. \quad (20)$$

Proof: The proof appears in Appendix B. ■

The MSE in (18) does not require matrix inversion and is only a function of the scalar variables: n_a , n_q , ρ_a , ρ_q , σ_a^2 , and σ_q^2 . Thus, it can be used to solve various optimization problems. The two extreme cases of Theorem 1 are when $n_a = 0$ and when $n_q = 0$. For these cases, substituting $n_a = 0$ in (18), we obtain

$$MSE = M - \frac{2M\rho_q n_q}{\pi(\rho_q + \sigma_q^2)(\alpha + (1 - \alpha)n_q)}. \quad (21)$$

Similarly, substituting $n_q = 0$ in (18), we obtain

$$MSE = M - \frac{M\rho_a n_a}{\rho_a n_a + \sigma_a^2}. \quad (22)$$

In both cases, the MSE given in (21) and (22) is a monotonically decreasing function of n_q and n_a , respectively. The expression in (21) coincides with the result in [10] for purely quantized data.

B. Constraints

Physical distributed networks, such as sensor networks, typically suffer from energy constraints and limited communication bandwidth, requiring quantization before data can be transmitted to a fusion center for further processing. In this context, one of the incentives of integrating low-resolution ADCs is their power consumption, which is much lower than that of high-resolution ADCs. In particular, power consumed in each ADC can be expressed as a factor of the number of quantization bits, \tilde{b} , as follows:

$$P_{ADC} = \text{FOM}_W f_s 2^{\tilde{b}}, \quad (23)$$

where f_s is the sampling rate and FOM_W is Walden's figure-of-merit for evaluating the power efficiency with ADCs resolution and speed [20]. In this paper, the power consumption of a single high-resolution ADC with b bits is denoted by P_H and that of a single 1-bit ADC by P_L . Thus, the total power consumption of the N_a high-resolution measurements is $N_a P_H$ and for the N_q low-resolution measurements is $N_q P_L$. Due to power limits of physical systems, we consider that the following constraint is imposed on the total power:

$$N_a P_H + N_q P_L \leq P_{\max}. \quad (24)$$

Substituting the power consumption of each ADC from (23) with $\tilde{b} = b$ and $\tilde{b} = 1$ for the b -bit and 1-bit measurements, respectively, into (24), we obtain the constraint

$$2^b N_a + 2N_q \leq \tilde{P}_{\max}, \quad (25)$$

where $\tilde{P}_{\max} \triangleq P_{\max}/\text{FOM}_W f_s$ is the normalized maximum power. By substituting $N_a = Mn_a$ and $N_q = Mn_q$, from assumption A.2 and A.3 of the LGO model, (25) can be rewritten as

$$2^b M n_a + 2M n_q \leq \tilde{P}_{\max}. \quad (26)$$

It should be noted that while the constraint in (24) treats the high-resolution measurements as finite b -bit quantized data, the MSE in (18) is derived under the assumption of pure analog measurements. Therefore, the number of bits that are used to represent the high-resolution ADC, b , should be chosen such that the quantization error is negligible. In simulations, we demonstrate that by choosing b large enough, the approximation of analog measurements holds and the MSE from (18) is achieved by b -bit quantized data.

In addition to the power constraints in (25), systems may also have other physical constraints on the number of measurements. This can be due to system design or available workspace, such as a field in which sensors are deployed, requiring a minimal distance from each other to avoid interference. The optimization in the following section can be readily extended to incorporate such constraints.

C. Resource Allocation

In this subsection, we optimize the resource allocation of the LGO model using the analytical expression of the MSE derived in Subsection III-A as an objective function and imposing the constraints from Subsection III-B. We show that the integer programming problem from (12) can be solved in polynomial time. It should be noted that the expression of the MSE in (18) can be used as a tractable objective function for different optimization problems of the LGO mixed-resolution scheme.

Under assumptions A.1-A.3, the objective function, i.e. the MSE from (9), is now given by (18). In addition, since M is known, the decision variables can be changed to be n_a and n_q , using the relation $N_a = Mn_a$ and $N_q = Mn_q$. The minimization of the MSE in the following is conducted under the power constraint in Subsection III-B. Thus, applying the constraint from (26) and substituting (18) in (12), the minimum MSE problem under a power constraint is formulated as

$$\begin{aligned} \min_{n_a, n_q} \quad & M - M \left(\frac{\rho_a n_a}{\rho_a n_a + \sigma_a^2} \right. \\ & \left. + \frac{2\rho_q n_q \sigma_a^4}{\pi(\rho_q + \sigma_q^2)(\alpha + \beta(n_a)\rho_q n_q)(\rho_a n_a + \sigma_a^2)^2} \right) \\ \text{s.t.} \quad & \begin{cases} 2^b M n_a + 2M n_q \leq \tilde{P}_{\max} \\ n_a, n_q \in \mathbb{Z}_+ \end{cases} \end{aligned} \quad (27)$$

Solving the optimization problem in (27) no longer requires the inversion of \mathbf{C}_x . Moreover, the values n_a and n_q are no longer found in the matrix dimensions. Thus, (27) can be solved using a standard search approach or by a conventional relaxation approach. In this paper, we adopt the first option.

Proposition 1. *The optimization problem in (27) can be solved using a one-dimensional search over n_a , taking a set of discrete values*

$$n_a \in \left\{ 0, 1, \dots, \left\lfloor \frac{\tilde{P}_{\max}}{2^b M} \right\rfloor \right\} \quad (28)$$

where for each value of n_a , the value of n_q is chosen to

utilize maximum power, i.e.

$$n_q = \left\lfloor \frac{\tilde{P}_{\max} - 2^b M n_a}{2M} \right\rfloor. \quad (29)$$

Proof: The proof appears in Appendix C. \blacksquare

Based on Proposition 1, one can numerically evaluate the optimal value, n_a^* , by using a simple one-dimensional search algorithm over the discrete values of n_a described in (28) to minimize the MSE. Then, the optimal number of quantized measurements, n_q^* , is obtained by substituting $n_a = n_a^*$ in (29). The optimal resource allocation depends on the system parameters: the total energy budget \tilde{P}_{\max} and the noise variances, σ_a^2 and σ_q^2 .

In the following we present a few special cases to interpret the MSE in (18) and the resource allocation optimization in (27).

- For the trivial case where the noise of the analog measurements approaches zero, i.e. $\sigma_a^2 \rightarrow 0$, it can be seen that the MSE in (18) approaches zero as well for any $n_a \geq 1$. Therefore, in this case an optimal solution of (27) is obtained for $n_a^* = 1$, which enables the estimation of θ without an estimation error such that the MSE is no longer a function of n_q . That is, additional measurements, both analog and quantized, won't change the optimal MSE value.
- For the case where the noise of the quantized measurements approaches zero, i.e. $\sigma_q^2 \rightarrow 0$, the parameter α , defined in (19), also approaches zero. By substituting $\sigma_q^2 \rightarrow 0$ and $\alpha \rightarrow 0$ in (18), we obtain that the MSE in this case is given by

$$\begin{aligned} \lim_{\sigma_q \rightarrow 0} \text{MSE} = M - M \left(\frac{\rho_a n_a}{\rho_a n_a + \sigma_a^2} \right. \\ \left. + \frac{2\sigma_a^4}{\pi(\rho_a n_a + \sigma_a^2)^2 - 2\rho_a n_a(\rho_a n_a + \sigma_a^2)} \right), \end{aligned} \quad (30)$$

for $n_q \geq 1$ and by (22) for $n_q = 0$. Depending on the available power, \tilde{P}_{\max} , the optimal resource allocation scheme in this case is determined. It can be seen that for $n_q \geq 1$, the MSE given in (30) is a constant function w.r.t. n_q . That is, for the noiseless case, the number of quantized measurements does not change the MSE as long as there is at least a single quantized measurement. Therefore, for this case of $\sigma_q \rightarrow 0$, the optimal policy in the sense of minimum MSE of the LMMSE estimator is one of the two following options: 1) take the maximum possible number of analog measurements and at least a single quantized measurement or 2) use only analog measurements, i.e. $n_{a_{\max}} \triangleq \left\lfloor \frac{\tilde{P}_{\max}}{2^b M} \right\rfloor$, as given in (22). The choice between these two options is as follows. If the available power maintains the following inequality

$$\tilde{P}_{\max} - \left\lfloor \frac{\tilde{P}_{\max}}{2^b M} \right\rfloor 2^b M \geq 2M \quad (31)$$

then Option 1 is the optimal solution of (27) for this case. If the inequality in (31) does not hold, the optimal solution is either Option 1 with $n_a^* = n_{a_{\max}} - 1$ and

$n_q^* \geq 1$ or Option 2 with $n_a^* = n_{a_{max}}$ and $n_q^* = 0$. Comparing the MSE in (22) and (30) for the latter case, Option 2 is optimal if the following inequality holds

$$((\pi - 2)\rho_a^2 - 2\rho_a\sigma_a^2) n_{a_{max}} > 2\sigma_a^4 - \pi\rho_a\sigma_a^2 + (\pi - 2)\rho_a^2 \quad (32)$$

and if not, then Option 1 is optimal. Thus, the sampling policy in this case depends on the noise variance of the analog measurement, σ_a^2 , the factor ρ_a , and the maximum number of available analog measurements under the power constraint from (24), i.e. by the condition in (31).

D. Optimization with Dithering

Dither, roughly speaking, is a random noise process added to a signal prior to its quantization [22], [34], [35]. The addition of dithering noise is commonly used in both Bayesian and non-Bayesian estimation with low-resolution quantized data. Although noise commonly degrades the performance of a system, it has been shown that the addition of noise to quantized measurements can improve system performance.

In this subsection, we consider the addition of independent, zero-mean, complex Gaussian dithering noise vectors, $\mathbf{w}_{d_a} \sim \mathcal{CN}(\mathbf{0}, \sigma_{d_a}^2 \mathbf{I}_{N_a})$ and $\mathbf{w}_{d_q} \sim \mathcal{CN}(\mathbf{0}, \sigma_{d_q}^2 \mathbf{I}_{N_q})$, to the analog and quantized measurements, respectively, before quantization. The dithering noise vectors, \mathbf{w}_{d_a} and \mathbf{w}_{d_q} , and the vectors $\boldsymbol{\theta}$, \mathbf{w}_a , and \mathbf{w}_q are assumed to be mutually independent. Therefore, the analog measurement vector in (2) now equals

$$\mathbf{x}_a = \mathbf{H}\boldsymbol{\theta} + \mathbf{w}_a + \mathbf{w}_{d_a}, \quad (33)$$

and the quantized measurement vector in (3) satisfies

$$\mathbf{x}_q = \mathcal{Q}(\mathbf{G}\boldsymbol{\theta} + \mathbf{w}_q + \mathbf{w}_{d_q}). \quad (34)$$

Since the vectors $\boldsymbol{\theta}$, \mathbf{w}_{d_a} , \mathbf{w}_{d_q} , \mathbf{w}_a , and \mathbf{w}_q are all mutually independent, then it can be shown, similar to the derivation of (4) and (6), that (33) and (34) imply, in this case, the following covariance matrices of the measurements:

$$\mathbf{C}_{\mathbf{x}_a} = \mathbf{H}\boldsymbol{\Sigma}_\theta\mathbf{H}^H + (\sigma_a^2 + \sigma_{d_a}^2)\mathbf{I}_{N_a} \quad (35)$$

and

$$\mathbf{C}_y = \mathbf{G}\boldsymbol{\Sigma}_\theta\mathbf{G}^H + (\sigma_q^2 + \sigma_{d_q}^2)\mathbf{I}_{N_q}. \quad (36)$$

Thus, all of the results developed in Subsections III-A and III-C hold with the noise variance of the analog measurements, σ_a^2 , increasing by $\sigma_{d_a}^2$, and that of the quantized measurements, σ_q^2 , increasing by $\sigma_{d_q}^2$. In particular, the MSE for the LGO model from (18) in this case is given by

$$MSE_{\hat{\theta}} = M - M \left(\frac{\rho_a n_a}{\rho_a n_a + \sigma_a^2 + \sigma_{d_a}^2} + \frac{2\rho_q n_q (\sigma_a^2 + \sigma_{d_a}^2)^2}{\pi(\rho_q + \sigma_q^2 + \sigma_{d_q}^2)(\alpha_d + \beta_d(n_a)\rho_q n_q)(\rho_a n_a + \sigma_a^2 + \sigma_{d_a}^2)^2} \right) \quad (37)$$

where

$$\alpha_d \triangleq \frac{2}{\pi} \arccos \left(\frac{\rho_q}{\rho_q + \sigma_q^2 + \sigma_{d_q}^2} \right) \quad (38)$$

and

$$\beta_d(n_a) \triangleq \frac{2}{\pi} \arcsin \left(\frac{\rho_q}{\rho_q + \sigma_q^2 + \sigma_{d_q}^2} \right) \frac{1}{\rho_q} - \frac{2\rho_a n_a}{\pi(\rho_q + \sigma_q^2 + \sigma_{d_q}^2)(\rho_a n_a + \sigma_a^2 + \sigma_{d_a}^2)}, \quad (39)$$

are the equivalent of (19) and (20), respectively, and replacing σ_a^2 and σ_q^2 with $\sigma_a^2 + \sigma_{d_a}^2$ and $\sigma_q^2 + \sigma_{d_q}^2$, respectively.

Under this model, the goal is to find the optimal resource allocation, the number of analog and quantized measurements, which minimizes the estimator's MSE while also optimizing the variance of the added dithering noise. Therefore, we look at the LGO Model from Subsection III-A and solve the optimization problem given in (27) with the objective function now being the MSE from (37) and adding the dithering noise variances, $\sigma_{d_a}^2$ and $\sigma_{d_q}^2$, as additional decision variables. Mathematically, the optimization problem in (27) with the addition of dithering noise can be rewritten as

$$\begin{aligned} \min_{n_a, n_q, \sigma_{d_a}^2, \sigma_{d_q}^2} \quad & M - M \left(\frac{\rho_a n_a}{\rho_a n_a + \sigma_a^2 + \sigma_{d_a}^2} + \frac{2\rho_q n_q (\sigma_a^2 + \sigma_{d_a}^2)^2}{\pi(\rho_q + \sigma_q^2 + \sigma_{d_q}^2)(\alpha_d + \beta_d(n_a)\rho_q n_q)(\rho_a n_a + \sigma_a^2 + \sigma_{d_a}^2)^2} \right) \\ \text{s.t.} \quad & \begin{cases} 2^b M n_a + 2M n_q \leq \tilde{P}_{max} \\ n_a, n_q \in \mathbb{N}_0 \\ \sigma_{d_a}^2 \geq 0 \\ \sigma_{d_q}^2 \geq 0 \end{cases}, \end{aligned} \quad (40)$$

where α_d and β_d are given in (38) and (39), respectively.

It can be shown that for any given set of values n_a , n_q , and $\sigma_{d_q}^2$ the optimal dither noise added to the analog measurements, $\sigma_{d_a}^2$, is zero. This solution is intuitive since for analog data, the MSE decreases as the signal-to-noise ratio (SNR) increases, and, thus, the addition of a dithering noise can only degrade estimation performance. Therefore, in the following, we discuss two scenarios of dithering: 1) the optimal solution, which is obtained by adding dithering noise to the quantized measurements only; and 2) adding dithering noise with the same variance to the entire system, both analog and quantized measurements. Thus, we add a single decision variable to the optimization problem in (40), denoted as σ_d^2 , where for Scenario 1 we set $\sigma_{d_a}^2 = 0$ and $\sigma_{d_q}^2 = \sigma_d^2$, and for Scenario 2 we set $\sigma_{d_a}^2 = \sigma_{d_q}^2 = \sigma_d^2$.

Similar to the derivation of Proposition 1, it can be proved that for each value of n_a and given the dithering noise variances, $\sigma_{d_a}^2$ and $\sigma_{d_q}^2$, the number of quantized measurements, n_q , should be chosen to be the maximum allowed under the power constraint. Works that utilize dithering, such as [13], [37], find the optimal dithering variance by using an exhaustive search. Similarly, we find the optimal allocation with dithering, i.e. the solution of (40), by utilizing a two-dimensional search over each value pair, n_a and n_q , while utilizing maximum power and for each pair search possible values of dithering variance σ_d^2 . This algorithm is summarized in Algorithm 1.

Algorithm 1: Resource Allocation with Dithering

Input: $M, b, \tilde{P}_{max}, \sigma_{d_{max}}^2, \sigma_{d_{res}}^2$
Output: $n_a^*, n_q^*, \sigma_d^{2*}$
Initialize $MSE_{opt} = M$
for $n_a = 0 : \lfloor \frac{\tilde{P}_{max}}{2^b M} \rfloor$ **do**
 $n_q = \lfloor \frac{\tilde{P}_{max} - 2^b M n_a}{2M} \rfloor$
 for $\sigma_d^2 = 0 : \sigma_{d_{res}}^2 : \sigma_{d_{max}}^2$ **do**
 Calculate MSE_{temp} by substituting $n_a, n_q,$
 and σ_d^2 in (37)
 if $MSE_{temp} < MSE_{opt}$ **then**
 Update optimal values: $MSE_{opt}, n_a^*, n_q^*,$
 σ_d^{2*} .
 end
 end
end

IV. SPECIAL CASES

In this section we discuss two special cases of the LGO model, described in Subsection III-C. In Subsection IV-A, we present the problem of estimating a scalar parameter from noisy measurements, a model which is widely used in WSN, for example [1], [22]. In Subsection IV-B, we discuss the allocation of analog and quantized measurements for channel estimation in massive MIMO communication systems [10], [15], [31], [38]–[40].

A. Estimation of a Scalar Parameter

In this subsection, we are interested in estimating a scalar unknown parameter, $\theta \in \mathbb{C}$, with a zero-mean complex Gaussian distribution, $\theta \sim \mathcal{CN}(0, 1)$, based on mixed-resolution data. Suppose, for example, a WSN with N sensors, where N_a of them transmit analog measurements and N_q transmit 1-bit quantized measurements, where $N = N_a + N_q$, to a central unit for estimation. In the case, (2) and (3) are reduced to

$$\mathbf{x}_a = \mathbf{1}_{N_a} \theta + \mathbf{w}_a \quad (41)$$

and

$$\mathbf{x}_q = \mathcal{Q}(\mathbf{1}_{N_q} \theta + \mathbf{w}_q), \quad (42)$$

respectively. We assume that \mathbf{w}_a and \mathbf{w}_q are independent, zero-mean complex Gaussian noise distributed $\mathbf{w}_a \sim \mathcal{CN}(\mathbf{0}, \sigma^2 \mathbf{I}_{N_a})$ and $\mathbf{w}_q \sim \mathcal{CN}(\mathbf{0}, \sigma^2 \mathbf{I}_{N_q})$. This scalar estimation problem satisfies the LGO model assumptions: First, it can be seen that the distribution of the unknown parameter, $\theta \sim \mathcal{CN}(0, 1)$, satisfies A.1). Second, $\mathbf{H} = \mathbf{1}_{N_a}$ and $\mathbf{G} = \mathbf{1}_{N_q}$ can be treated as block matrices with each entry being the scalar 1, which in turn satisfies assumption A.2) and A.3) with $\rho_a = 1$ and $\rho_q = 1$. Satisfying the assumptions allows us to use Theorem 1 in order to find the optimal measurement allocation scheme for the scalar case. It should be noted that since the dimensions of the auto-covariance matrix \mathbf{C}_x are affected by the number of measurements, N_a and N_q , and not by the size of the unknown parameter vector θ . Solving the optimization problem in (12) still requires the inversion of \mathbf{C}_x at each value pair for the scalar case. Therefore, the proposed

tractable formulation in (27) is also relevant and important for the scalar case.

B. Channel Estimation in Massive MIMO

In this subsection, we consider the special case of channel estimation using analog and 1-bit quantized measurement in massive MIMO networks. Massive MIMO has a high potential of enabling technology beyond fourth generation (5G) cellular systems due to its advantages in terms of spectral efficiency, energy efficiency, and the ability to use low-cost low-power hardware [41], [42]. The following model of mixed-ADC massive MIMO has been used in [10], [15], [31], [38]–[40] and is described in detail due to its importance and to clarify the relation to the considered LGO model.

We study the uplink of a single-cell multi-user MIMO system consisting of K single antenna users transmitting independent data symbols simultaneously to a base station (BS) equipped with L antennas. We consider a block-fading model with coherence bandwidth W_c and coherence time T_c . In this model, each channel remains constant in a coherence interval of length $T = T_c W_c$ symbols and changes independently between intervals. The coherence interval can be divided into two parts: the first part is used for channel estimation, referred to as the training phase, while the second part is for data transmission. During training, all K users simultaneously transmit their pilot sequences of K mutually orthogonal pilot symbols. Therefore, the received signal during the training phase is

$$\mathbf{R} = \sqrt{\rho} \mathbf{A} \Phi^T + \mathbf{W}, \quad (43)$$

where $\mathbf{A} \in \mathbb{C}^{L \times K}$ is the channel matrix, ρ is the pilot transmission power, $\Phi \in \mathbb{C}^{K \times K}$ is the pilot signal matrix transmitted from the K users, and \mathbf{W} is independent, zero-mean, complex Gaussian noise with each element distributed $\mathcal{CN}(\mathbf{0}, \sigma^2)$. We assume the channel vectors are i.i.d. and denote the l th row of \mathbf{A} as \mathbf{a}_l , where \mathbf{a}_l has a zero-mean complex Gaussian distribution, i.e. $\mathbf{a}_l \sim \mathcal{CN}(\mathbf{0}, \mathbf{I}_K)$. The pilot sequences are drawn from the pilot signal matrix Φ , where $\Phi^H \Phi = \mathbf{I}_K$.

Since we assume independent channels and noise, then the rows of \mathbf{R} from (43) are mutually independent, enabling us to analyze each row separately. Therefore, the l th row of \mathbf{R} (viewed as a column vector), satisfies

$$\mathbf{r}_l = \sqrt{\rho} \Phi \mathbf{a}_l + \mathbf{w}_l, \quad l = 1, \dots, L. \quad (44)$$

Due to the high power consumption of high-resolution ADCs and the less informative data of low-resolution ADCs, in many works both analog and quantized measurements are used to benefit from both worlds (see, e.g. [12], [13] and references therein). In order to achieve good performance there is a need for more measurements when working with quantized data as opposed to analog. Therefore, the pilot sequence, Φ , can be transmitted a number of times with the antennas switching between the high- and low-resolution ADCs at each transmit.

Let us transmit the K pilot symbols N times. For each channel $l \in \{1, \dots, L\}$, we denote the number of times the pilot sequence is transmitted with the analog ADC connected to the antenna as n_{a_l} and with the 1-bit quantized ADC as

n_{q_l} where $n_{a_l} + n_{q_l} = N$. We can organize the measurements now such that the analog measurements from (44) are

$$\mathbf{r}_{a_l} = \sqrt{\rho} \Phi_a \mathbf{a}_l + \mathbf{w}_a, \quad (45)$$

where $\mathbf{r}_{a_l} \in \mathbb{C}^{n_{a_l} K}$ and Φ_a is a $n_{a_l} K \times K$ block matrix defined as

$$\Phi_a = \mathbf{1}_{n_a} \otimes \Phi. \quad (46)$$

Similarly, the quantized measurements from (44) are

$$\mathbf{r}_{q_l} = \sqrt{\rho} \Phi_q \mathbf{a}_l + \mathbf{w}_q, \quad (47)$$

where $\mathbf{r}_{q_l} \in \mathbb{C}^{n_{q_l} K}$ and Φ_q is a $n_{q_l} K \times K$ block matrix defined as

$$\Phi_q = \mathbf{1}_{n_q} \otimes \Phi. \quad (48)$$

By setting $\mathbf{a}_l = \boldsymbol{\theta}$, $\mathbf{r}_{a_l} = \mathbf{x}_a$, and $\mathbf{r}_{q_l} = \mathbf{x}_q$ the measurement model in (45) and (47) coincides with the general measurement model in (2) and (3) where $M = K$. Moreover, we now show that Assumptions A.1-A.3 from Subsection III-A are satisfied for the mixed-ADC massive MIMO model. First, the channel is modeled such that $\mathbf{a}_l \sim \mathcal{CN}(\mathbf{0}, \mathbf{I}_M)$ keeping the assumption that $\boldsymbol{\Sigma}_\theta = \mathbf{I}_M$. Thus, Assumption A.1) is satisfied. Second, by using (45) and (46), it can be seen that the matrix $\mathbf{H} = \sqrt{\rho} \Phi_a$ is a block matrix of size $n_{a_l} K \times K$ and satisfies $(\sqrt{\rho} \Phi_a)^H \sqrt{\rho} \Phi_a = \rho \mathbf{I}_K$, thus Assumption A.2) is satisfied with $\rho_a = \rho$. Similarly, by using (47) and (48), it can be seen that the matrix $\mathbf{G} = \sqrt{\rho} \Phi_q$ satisfies Assumption A.3) with $\rho_q = \rho$.

The goal under this model is to estimate the channel of a system consisting of a single antenna, $L = 1$, while using both a high- and low-resolution ADCs in the BS, which the antenna can switch between to acquire both analog and quantized measurements. The number of measurements taken, or equivalently the number of times the pilot signal is transmitted using each ADC resolution, is to be optimized to minimize the MSE of the LMMSE estimator, while not exceeding the power consumption at the BS. Substituting $M = K$, $\rho_a = \rho_q = \rho$, and $\sigma_a^2 = \sigma_q^2 = \sigma^2$ in (27), the resource allocation problem can be solved for the problem of channel estimation in massive MIMO systems. Similarly, the same substitution can be done in (40) allowing to find the optimal resource allocation with dithering.

This approach can be extended to the more general case, where there are $L \geq 1$ i.i.d. antennas or channels to estimate. The channel estimation problem for the channel (43) can be decomposed into parallel estimation problems [30] solved separately for each channel with the maximum power available equaling for example, to P_{max}/L , allocating each channel an equal power supply, thus allowing us to optimize the whole system while solving the problem for a single channel.

V. SIMULATIONS

In this section we numerically evaluate the performance of the mixed-resolution system presented in Section III and that of the proposed resource allocation optimization approach. In Subsection V-A we simulate the scalar case from Subsection IV-A, in Subsection V-A we simulate the model of channel estimation in massive MIMO from Subsection IV-B, and in Subsection V-C we compare the run time of the proposed

resource allocation approach and the brute-force approach in (12). As discussed in Subsection III-B, in order for the quantization noise to be negligible we use $b = 6$ bits on a quantization range $[-5, 5]$ to represent our analog measurements. The noise added to the analog and quantized measurements is assumed to have the same variance, $\sigma_a^2 = \sigma_q^2 = \sigma^2$, and we set $\rho_a = \rho_q = 1$. Our results are averaged over 100 Monte-Carlo simulations.

A. Scalar Parameter Estimation

In this subsection, estimation of a scalar parameter, $M = 1$, as discussed in Subsection IV-A, is evaluated. The simulation results in Fig. 2 show the behavior of the MSE from (18) for the scalar case with different values of n_a and n_q as a function of the noise variance σ^2 . It can be seen that the addition of measurements, be it analog or quantized, does not degrade the performance in terms of MSE. In addition, when only analog measurements are used, $n_q = 0$, the MSE monotonically decreases as σ^2 decreases. The same can not be said for the mixed-resolution case for which the behavior of the MSE is not even convex. For example, it can be seen that there are cases such as $n_a = 1$ and $n_q = 100$ that the addition of dithering noise to both measurement types can improve the MSE which may be counterintuitive due to the behavior of pure analog measurement estimation. In Fig. 3a and Fig. 3b,

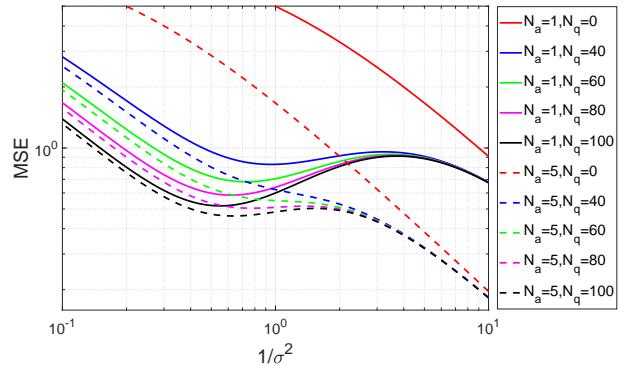


Fig. 2: Scalar case: effects of noise variance on the estimator's MSE for different number of measurements.

the MSE is shown for a given noise variance, σ^2 , as a function of the number of analog measurements, n_a , and quantized measurements, n_q . Dots on the graphs show the possible value pairs of analog and quantized measurements, n_a and n_q , for different values of available power, \bar{P}_{max} . These figures show, as before, that taking more measurements does not increase the MSE. In addition, it can be seen that using a mixed-resolution approach can have a lower MSE than assuming a naive approach which utilizes only one type of measurement up to the maximum power available.

B. Channel Estimation in Massive MIMO

In this subsection, the massive MIMO model, as described in Subsection IV-B, is simulated. The resource allocation optimization problem in (27) is solved for $M = 10$ users

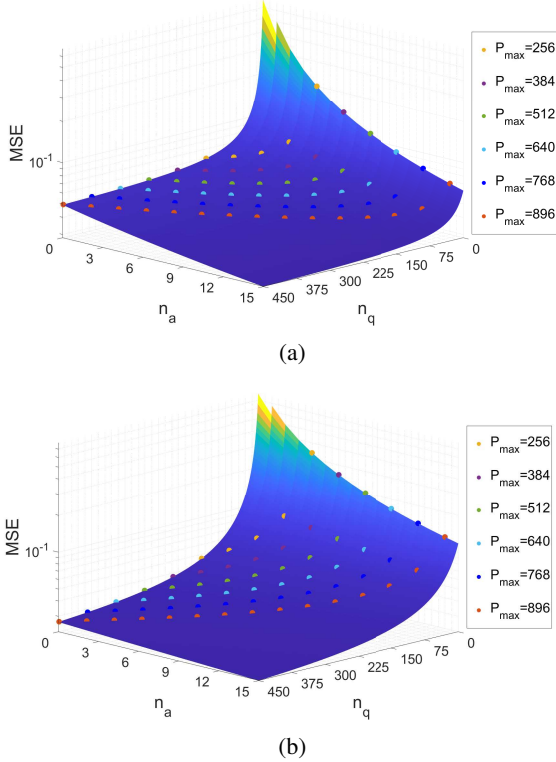


Fig. 3: Scalar Case: The MSE as a function of the number of analog and quantized measurements, n_a and n_q . The noise variance is $\sigma^2 = 1$ (a) and $\sigma^2 = 2$ (b), where $\sigma^2 = \sigma_a^2 = \sigma_q^2$.

transmitting a randomly generated pilot matrix Φ . The maximum power available is set to $\tilde{P}_{max} = 2^b M n_{a,max}$, where $b = 6$ and $n_{a,max} = 20$. In Fig. 4 we compare between the optimal resource allocation calculated using a one-dimensional search, as described in Subsection III-C, and between two naive solutions: 1) a greedy scheme, which utilizes the maximum number of analog measurements and 2) a cost-effective scheme, which uses the maximum number of measurements by only having quantized measurements. The analytic MSE is calculated under the assumption of pure analog measurements, i.e. as given in (27), although we use in practice $b = 6$ -level quantized data. Therefore, we also present Monte-Carlo simulations of the obtained MSE in practice that show that the values to represent the analog measurements make the quantization noise negligible for the purpose of estimation.

We can divide the graph into three sections: 1) low noise variance, $\sigma^2 < 0.2$, in which case the use of all analog measurements is optimal, 2) high noise variance, $\sigma^2 > 2$, in which the use of all quantized measurements is optimal, and 3) middle section, $0.2 < \sigma^2 < 2$, in which it is optimal to use a mixed-resolution measurement scheme. Moreover, Fig. 4 also compares the aforementioned solutions to the solution of the resource allocation optimization problem with optimization of the dithering noise added only to the quantized measurements. This is done using a two-dimensional search over n_a and σ_{qd}^2 with $\sigma_{qd}^2 \in [0, 2]$ with increments of 0.1, as in Algorithm 1. In the middle section in which better performance was achieved by using the mixed-resolution scheme as opposed to

the naive solutions, the addition of dithering noise improved performance even more. As expected, in the low noise variance section, in which the analog measurements are optimal, the dithering had no effect but it did effect part of the high noise variance section improving the performance when using all quantized measurement. Therefore, we can conclude that utilizing dithering can improve system performance in the sense of the LMMSE estimator's MSE.

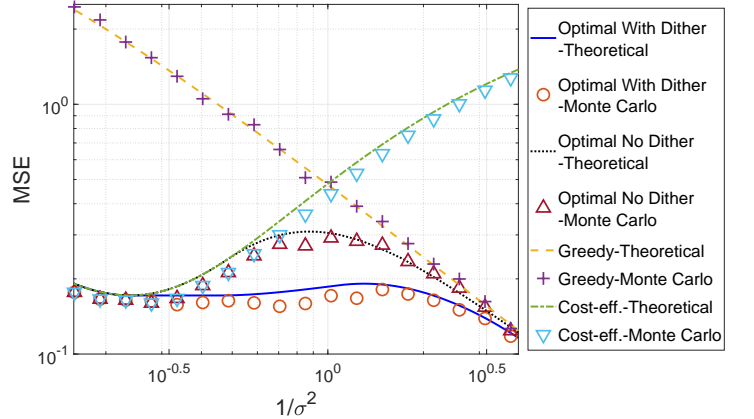


Fig. 4: Channel estimation in massive MIMO with $M = 10$ users. The MSE of the LMMSE estimator versus the noise variance, where $\sigma^2 = \sigma_a^2 = \sigma_q^2$. The addition of dithering noise is available only to the 1-bit quantized measurements in the mixed-resolution scheme.

C. Run Time

In this subsection, the computational complexity of solving the resource allocation optimization problem is evaluated under the LGO measurement model. This is done by comparing the time of solving the optimization problem in (12) using the closed-form analytic expression of the MSE derived in Theorem 1 compared to the general MSE term in (9), which requires matrix inversion. In both cases, the one-dimensional search from Proposition 1 is used. It should be noted that the general MSE term in (9) does not give insight on the behavior of the MSE. Therefore, Proposition 1 isn't proven for the general term which in turn requires a two-dimensional search over all possible value pairs of n_a and n_q in order to solve the resource allocation optimization problem. Thus, for the general case, the run time of the optimization problem using the general MSE term is much longer than that presented in the simulation. The average computation time, run time, was evaluated by running the algorithm using Matlab on an Intel Xeon E5-2660 CPU. In Fig. 5 we show the run time of the optimal resource allocation in both forms of the MSE as a function of the maximum number of analog measurements available. The maximum power available is set to equal $\tilde{P}_{max} = 2^b M n_{a,max}$ and we evaluate the cases of $M = 1, 3, 10$. It can be seen that the more analog measurements are available, the larger the maximum power and therefore, the computation time increases since the search is over more values. This has a larger effect when using matrix

inversion since $\mathbf{C}_x \in \mathbb{C}^{(n_a+n_q)M \times (n_a+n_q)M}$. In addition, the size of the unknown parameter vector, $\theta \in \mathbb{C}^M$, does not affect the run time of the proposed approach in Theorem 1 while increasing the calculation time of the matrix inversion MSE in the direct approach.

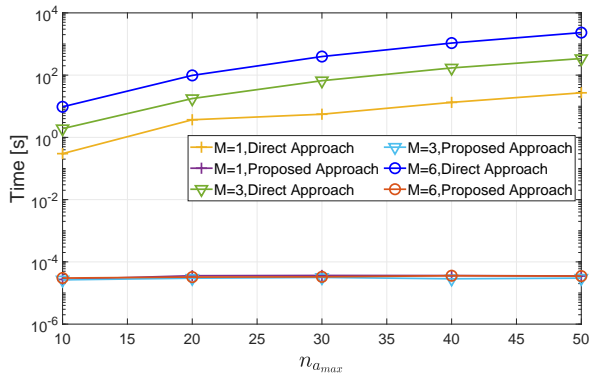


Fig. 5: Run time comparison between calculation of the MSE using the direct approach and the closed-form expression in Theorem 1 for different values of M .

VI. CONCLUSION

In this paper, we consider Bayesian parameter estimation using mixed-resolution measurements. First, we derive the LMMSE estimator and its associated MSE for the mixed-resolution case. It is shown that the MSE requires matrix inversion with the size of the matrix depending on the number of analog and quantized measurements, and thus, optimization problems that aim to minimize the MSE w.r.t. the number of measurements are impractical due to the exhaustive search required. Next, we present the LGO model for which we calculate a closed-form expression for the LMMSE estimator and its corresponding MSE. Two special cases for which the mixed-resolution scheme under the LGO model is relevant are presented: 1) scalar parameter estimation which is used, for example, in WSN, and 2) channel estimation in massive MIMO communication systems. Based on the closed-form expression of the MSE and enforcing a power consumption constraint, a resource allocation optimization problem is formulated with the goal of finding the optimal resources, namely the number of analog and quantized measurements. A one-dimensional search is proven to be sufficient in finding the optimal solution to the problem. Furthermore, the concept of dithering is presented and the resource allocation optimization problem is derived while also allowing optimization of the dithering noise variance added to the system. Finally, in the simulations we show that the mixed-resolution scheme outperforms the naive approaches of pure analog or pure quantized measurements for certain ranges of noise variance that are not in the asymptotic region nor the so-called non-informative region. In addition, the possible benefits of dithering on estimation performance in terms of MSE are shown for mixed-resolution schemes. Solving the resource allocation optimization problem for the LGO measurement model has a low-complexity solution allowing fast calculation. The mixed-resolution scheme can and

should be adopted in different real-world applications with the solution for the LGO measurement model easily achieved and thus improve system performance.

APPENDIX A DERIVATION OF (10) AND (11)

In this appendix we develop the auto-covariance and cross-covariance matrices from (10) and (11) for the general model described in Subsection II-A. By using (7), it can be verified that the auto-covariance and cross-covariance matrices are block matrices given by

$$\mathbf{C}_x = \begin{bmatrix} \mathbf{C}_{x_a} & \mathbf{C}_{x_a x_q} \\ \mathbf{C}_{x_q x_a} & \mathbf{C}_{x_q} \end{bmatrix} \quad (49)$$

and

$$\mathbf{C}_{\theta x} = [\mathbf{C}_{\theta x_a} \quad \mathbf{C}_{\theta x_q}], \quad (50)$$

respectively, where \mathbf{C}_{x_a} is given in (4). From the analog measurement vector \mathbf{x}_a given in (2) and based on the measurement model in Subsection II-A, it can be verified that

$$\mathbf{C}_{\theta x_a} = \Sigma_{\theta} \mathbf{H}^H. \quad (51)$$

To calculate the covariance matrix \mathbf{C}_{x_q} we use the arcsine law (p. 396 in [43]) which implies that given two zero-mean jointly complex Gaussian random variables, r and t , the cross-covariance of the quantized variables, $\mathcal{Q}(r)$ and $\mathcal{Q}(t)$, is given by

$$\begin{aligned} \mathbf{C}_{\mathcal{Q}(r), \mathcal{Q}(t)} &= \mathbb{E}[\mathcal{Q}(r)\mathcal{Q}^*(t)] \\ &= \frac{2}{\pi} \left[\arcsin \left(\frac{\text{Re}\{\mathbf{C}_{rt}\}}{\sqrt{\sigma_t^2 \sigma_r^2}} \right) + j \arcsin \left(\frac{\text{Im}\{\mathbf{C}_{rt}\}}{\sqrt{\sigma_t^2 \sigma_r^2}} \right) \right], \end{aligned} \quad (52)$$

where σ_t^2 and σ_r^2 are the covariance of the random variables t and r , respectively. Therefore, given the measurement vector \mathbf{x}_q in (3), which is the 1-bit quantization of \mathbf{y} in (5), and applying the result in (52) element-wise, the auto-covariance matrix is given by

$$\begin{aligned} \mathbf{C}_{x_q} &= \mathbb{E}[\mathbf{x}_q \mathbf{x}_q^H] = \mathbb{E}[\mathcal{Q}(\mathbf{y}) \mathcal{Q}^H(\mathbf{y})] \\ &= \frac{2}{\pi} \left[\arcsin \left((\text{diag}(\mathbf{C}_y))^{-\frac{1}{2}} \text{Re}(\mathbf{C}_y) (\text{diag}(\mathbf{C}_y))^{-\frac{1}{2}} \right) \right. \\ &\quad \left. + j \arcsin \left((\text{diag}(\mathbf{C}_y))^{-\frac{1}{2}} \text{Im}(\mathbf{C}_y) (\text{diag}(\mathbf{C}_y))^{-\frac{1}{2}} \right) \right], \end{aligned} \quad (53)$$

where \mathbf{C}_y is defined in (6). It should be noted that the matrix \mathbf{C}_{x_q} in (53) is well defined according to the following explanation. The elements of the matrix

$$\left[(\text{diag}(\mathbf{C}_y))^{-\frac{1}{2}} \mathbf{C}_y (\text{diag}(\mathbf{C}_y))^{-\frac{1}{2}} \right]_{i,j} = \frac{\mathbf{C}_{y_i y_j}}{\sqrt{\mathbf{C}_{y_i} \mathbf{C}_{y_j}}}, \quad (54)$$

are, by definition, the Pearson correlation coefficients. Therefore, from the properties of the Pearson correlation coefficient,

$$\left| \frac{\mathbf{C}_{y_i y_j}}{\sqrt{\mathbf{C}_{y_i} \mathbf{C}_{y_j}}} \right| \leq 1, \quad (55)$$

and since $|\text{Re}(\mathbf{C}_{y_i y_j})| \leq |\mathbf{C}_{y_i y_j}|$ we obtain

$$\left| \frac{\text{Re}(\mathbf{C}_{y_i y_j})}{\sqrt{\mathbf{C}_{y_i} \mathbf{C}_{y_j}}} \right| \leq 1. \quad (56)$$

Similarly, the same holds for $\text{Im}(\mathbf{C}_{y_i y_j})$ and thus, the auto-covariance matrix $\mathbf{C}_{\mathbf{x}_q}$ in (53) is well defined.

Finally, to calculate the cross-covariance matrix of \mathbf{x}_q with $\boldsymbol{\theta}$ and \mathbf{x}_a we use the Bussgang Theorem [44], which implies that for two zero-mean complex Gaussian random variables, r and t , with 1-bit quantization as given in (1), the cross-covariance is given by

$$\mathbf{C}_{r\mathcal{Q}(t)} = \mathbb{E}[r\mathcal{Q}^*(t)] \sqrt{\frac{2}{\pi\sigma_t^2}} \mathbf{C}_{rt}, \quad (57)$$

where σ_t^2 is the covariance of the random variable t . Therefore, the cross-covariance matrix of $\boldsymbol{\theta}$ and \mathbf{x}_q is given by

$$\begin{aligned} \mathbf{C}_{\boldsymbol{\theta}\mathbf{x}_q} &= \mathbb{E}[\boldsymbol{\theta}\mathcal{Q}^H(\mathbf{y})] \\ &= \sqrt{\frac{2}{\pi}} \mathbb{E}[\boldsymbol{\theta}(\boldsymbol{\theta}^H \mathbf{G}^H + \mathbf{w}_q^H)] (\text{diag}(\mathbf{C}_y))^{-\frac{1}{2}} \\ &= \sqrt{\frac{2}{\pi}} \boldsymbol{\Sigma}_\theta \mathbf{G}^H (\text{diag}(\mathbf{C}_y))^{-\frac{1}{2}}, \end{aligned} \quad (58)$$

where the second equality is obtained by implementing the Bussgang formula from (57) element-wise, and the last equality following the fact that $\boldsymbol{\theta}$ and \mathbf{w}_a are mutually independent and \mathbf{G} is deterministic. Similarly, from (57) and due to the fact that \mathbf{w}_a , \mathbf{w}_q , and $\boldsymbol{\theta}$ are mutually independent, the cross-covariance of \mathbf{x}_a and \mathbf{x}_q is given by

$$\begin{aligned} \mathbf{C}_{\mathbf{x}_a\mathbf{x}_q} &= \mathbb{E}[\mathbf{x}_a \mathcal{Q}(\mathbf{y})^H] \\ &= \sqrt{\frac{2}{\pi}} \mathbb{E}[(\mathbf{H}\boldsymbol{\theta} + \mathbf{w}_a^H)(\boldsymbol{\theta}^H \mathbf{G}^H + \mathbf{w}_q^H)] (\text{diag}(\mathbf{C}_y))^{-\frac{1}{2}} \text{ and} \\ &= \sqrt{\frac{2}{\pi}} \mathbf{H}\boldsymbol{\Sigma}_\theta \mathbf{G}^H (\text{diag}(\mathbf{C}_y))^{-\frac{1}{2}}. \end{aligned} \quad (59)$$

By substituting (51), (53), (58), and (59) in (49) and (50) we obtain that the auto-covariance and cross-covariance matrices are given by (10) and (11), respectively.

APPENDIX B PROOF OF THEOREM 1

In this appendix we prove that the LMMSE estimator from (8) and its MSE from (9) are reduced, under Assumptions A.1-A.3, to (17) and (18), respectively. By substituting $\boldsymbol{\Sigma}_\theta = \mathbf{I}_M$ from Assumption A.1 in (4), (6), and (51) we obtain that in this case the auto-covariance and cross-covariance matrices satisfy

$$\mathbf{C}_{\mathbf{x}_a} = \mathbf{H}\mathbf{H}^H + \sigma_a^2 \mathbf{I}_{N_a}, \quad (60)$$

$$\mathbf{C}_y = \mathbf{G}\mathbf{G}^H + \sigma_q^2 \mathbf{I}_{N_q}, \quad (61)$$

and

$$\mathbf{C}_{\boldsymbol{\theta}\mathbf{x}_a} = \mathbf{H}^H. \quad (62)$$

By substituting (15) and (16) from Assumption A.3 in (61), we obtain

$$\mathbf{C}_y = \rho_q (\mathbf{1}_{n_q} \mathbf{1}_{n_q}^T) \otimes \mathbf{I}_M + \sigma_q^2 \mathbf{I}_{N_q}, \quad (63)$$

which is a real matrix. Thus, by applying the diagonal operator on \mathbf{C}_y in (63), one obtains

$$\text{diag}(\mathbf{C}_y) = (\rho_q + \sigma_q^2) \mathbf{I}_{N_q}, \quad (64)$$

and therefore,

$$(\text{diag}(\mathbf{C}_y))^{-\frac{1}{2}} = \frac{1}{\sqrt{\rho_q + \sigma_q^2}} \mathbf{I}_{N_q}. \quad (65)$$

From (63) and (65), we obtain that

$$\begin{aligned} (\text{diag}(\mathbf{C}_y))^{-\frac{1}{2}} \mathbf{C}_y (\text{diag}(\mathbf{C}_y))^{-\frac{1}{2}} &= \\ &= \mathbf{I}_{N_q} + \frac{\rho_q}{\rho_q + \sigma_q^2} ((\mathbf{1}_{n_q} \mathbf{1}_{n_q}^T) \otimes \mathbf{I}_M - \mathbf{I}_{N_q}). \end{aligned} \quad (66)$$

Substituting (66) in (53) we obtain

$$\mathbf{C}_{\mathbf{x}_q} = \frac{2}{\pi} \arcsin \left((\text{diag}(\mathbf{C}_y))^{-\frac{1}{2}} \text{Re}(\mathbf{C}_y) (\text{diag}(\mathbf{C}_y))^{-\frac{1}{2}} \right). \quad (67)$$

Applying the element-wise arcsin function on (66), results in

$$\begin{aligned} \mathbf{C}_{\mathbf{x}_q} &= \frac{2}{\pi} \left(\frac{\pi}{2} \mathbf{I}_{N_q} + \arcsin \left(\frac{\rho_q}{\rho_q + \sigma_q^2} \right) \left(\frac{1}{\rho_q} \mathbf{G}\mathbf{G}^H - \mathbf{I}_{N_q} \right) \right) \\ &= \alpha \mathbf{I}_{N_q} + (1 - \alpha) \frac{1}{\rho_q} \mathbf{G}\mathbf{G}^H, \end{aligned} \quad (68)$$

where α is defined in (19).

Substituting $\boldsymbol{\Sigma}_\theta = \mathbf{I}_M$, from Assumption A.1, and (65) into (59) and (58) we obtain:

$$\mathbf{C}_{\mathbf{x}_a\mathbf{x}_q} = \sqrt{\frac{2}{\pi(\rho_q + \sigma_q^2)}} \mathbf{H}\mathbf{G}^H \quad (69)$$

$$\mathbf{C}_{\boldsymbol{\theta}\mathbf{x}_q} = \sqrt{\frac{2}{\pi(\rho_q + \sigma_q^2)}} \mathbf{G}^H, \quad (70)$$

respectively. Substitution of (60), (68), (69), and (70) in (10) and (11) results in

$$\begin{aligned} \mathbf{C}_x &= \begin{bmatrix} \mathbf{C}_{\mathbf{x}_a} & \mathbf{C}_{\mathbf{x}_a\mathbf{x}_q} \\ \mathbf{C}_{\mathbf{x}_q\mathbf{x}_a} & \mathbf{C}_{\mathbf{x}_q} \end{bmatrix} \\ &= \begin{bmatrix} \mathbf{H}\mathbf{H}^H + \sigma_a^2 \mathbf{I}_{N_a} & \sqrt{\frac{2}{\pi(\rho_q + \sigma_q^2)}} \mathbf{H}\mathbf{G}^H \\ \sqrt{\frac{2}{\pi(\rho_q + \sigma_q^2)}} \mathbf{G}\mathbf{H}^H & \alpha \mathbf{I}_{N_q} + (1 - \alpha) \frac{1}{\rho_q} \mathbf{G}\mathbf{G}^H \end{bmatrix} \end{aligned} \quad (71)$$

and

$$\mathbf{C}_{\boldsymbol{\theta}\mathbf{x}} = \left[\mathbf{H}^H \quad \sqrt{\frac{2}{\pi(\rho_q + \sigma_q^2)}} \mathbf{G}^H \right], \quad (72)$$

respectively.

The auto-covariance matrix in (71) is a block matrix. Therefore in order to calculate its inverse, we first note that using the Woodbury matrix identity (Eq. (0.7.4.1) [45]) the inverse of the left upper block of \mathbf{C}_x , which is given in (60), satisfies

$$\begin{aligned} \mathbf{C}_{\mathbf{x}_a}^{-1} &= \frac{1}{\sigma_a^2} \left(\mathbf{I}_{N_a} - \frac{1}{\sigma_a^2} \mathbf{H} \left(\mathbf{I}_M + \frac{1}{\sigma_a^2} \mathbf{H}^H \mathbf{H} \right)^{-1} \mathbf{H}^H \right) \\ &= \frac{1}{\sigma_a^2} \left(\mathbf{I}_{N_a} - \frac{1}{\rho_a n_a + \sigma_a^2} \mathbf{H}\mathbf{H}^H \right). \end{aligned} \quad (73)$$

where the last equality is obtained from (13) and (14) in Assumption A.2 which implies that $\mathbf{H}^H \mathbf{H} = \rho_a n_a \mathbf{I}_M$. Second,

by using (68), (69), and (73), it can be verified that

$$\begin{aligned} \mathbf{C}_{\mathbf{x}_q} - \mathbf{C}_{\mathbf{x}_q \mathbf{x}_a} \mathbf{C}_{\mathbf{x}_a}^{-1} \mathbf{C}_{\mathbf{x}_a \mathbf{x}_q} &= \alpha \mathbf{I}_{N_q} + (1 - \alpha) \frac{1}{\rho_q} \mathbf{G} \mathbf{G}^H \\ &- \frac{2}{\pi(\rho_q + \sigma_q^2)} \frac{1}{\sigma_a^2} \mathbf{G} \mathbf{H}^H \left(\mathbf{I}_{N_a} - \frac{1}{\rho_a n_a + \sigma_a^2} \mathbf{H} \mathbf{H}^H \right) \mathbf{H} \mathbf{G}^H \\ &= \alpha \left(\mathbf{I}_{N_q} + \frac{\beta}{\alpha} \mathbf{G} \mathbf{G}^H \right) \triangleq \mathbf{D}, \end{aligned} \quad (74)$$

where β is defined in (20) and using $\mathbf{H}^H \mathbf{H} = \rho_a n_a \mathbf{I}_M$. By using the Woodbury matrix identity on (74), the inverse matrix is given by:

$$\begin{aligned} &(\mathbf{C}_{\mathbf{x}_q} - \mathbf{C}_{\mathbf{x}_q \mathbf{x}_a} \mathbf{C}_{\mathbf{x}_a}^{-1} \mathbf{C}_{\mathbf{x}_a \mathbf{x}_q})^{-1} \\ &= \frac{1}{\alpha} \left(\mathbf{I}_{N_q} - \frac{\beta}{\alpha} \mathbf{G} \left(\mathbf{I}_M + \frac{\beta}{\alpha} \mathbf{G}^H \mathbf{G} \right)^{-1} \mathbf{G}^H \right) \quad (75) \\ &= \frac{1}{\alpha} \left(\mathbf{I}_{N_q} - \frac{\beta}{\alpha + \beta \rho_q n_q} \mathbf{G} \mathbf{G}^H \right), \end{aligned}$$

where the last equality is obtained from (15) and (16) in Assumption A.3, which implies that $\mathbf{G}^H \mathbf{G} = \rho_q n_q \mathbf{I}_M$. Using block matrix inversion together with the results in (73) and (75), it can be verified that the inverse auto-covariance matrix in (71) is

$$\begin{aligned} \mathbf{C}_{\mathbf{x}}^{-1} &= \begin{bmatrix} \mathbf{C}_{\mathbf{x}_a}^{-1} + \mathbf{C}_{\mathbf{x}_a}^{-1} \mathbf{C}_{\mathbf{x}_a \mathbf{x}_q} \mathbf{D}^{-1} \mathbf{C}_{\mathbf{x}_q \mathbf{x}_a} \mathbf{C}_{\mathbf{x}_a}^{-1} & \vdots \\ -\mathbf{D}^{-1} \mathbf{C}_{\mathbf{x}_q \mathbf{x}_a} \mathbf{C}_{\mathbf{x}_a}^{-1} & \vdots \\ & -\mathbf{C}_{\mathbf{x}_a}^{-1} \mathbf{C}_{\mathbf{x}_a \mathbf{x}_q} \mathbf{D}^{-1} \\ & \mathbf{D}^{-1} \end{bmatrix} \\ &= \begin{bmatrix} \frac{1}{\sigma_a^2} (\mathbf{I}_{N_a} + \nu(n_a, n_q) \mathbf{H} \mathbf{H}^H) & \vdots \\ -\xi(n_a, n_q) \mathbf{G} \mathbf{H}^H & \vdots \\ & -\xi(n_a, n_q) \mathbf{H} \mathbf{G}^H \\ & \frac{1}{\alpha} \left(\mathbf{I}_{N_q} - \frac{\beta(n_a)}{\alpha + \beta(n_a) \rho_q n_q} \mathbf{G} \mathbf{G}^H \right) \end{bmatrix}, \end{aligned} \quad (76)$$

where

$$\begin{aligned} \nu(n_a, n_q) &\triangleq -\frac{1}{\rho_a n_a + \sigma_a^2} \\ &+ \frac{2\rho_q n_q \sigma_a^2}{\pi(\rho_q + \sigma_q^2)(\alpha + \beta(n_a) \rho_q n_q)(\rho_a n_a + \sigma_a^2)^2} \end{aligned} \quad (77)$$

and

$$\xi(n_a, n_q) \triangleq \sqrt{\frac{2}{\pi(\rho_q + \sigma_q^2)} \frac{1}{(\alpha + \beta(n_a) \rho_q n_q)(\rho_a n_a + \sigma_a^2)}}. \quad (78)$$

Substituting (72) and (76) into (8) and (9) we obtain (17) and (18), respectively.

APPENDIX C PROOF OF PROPOSITION 1

In this appendix we prove that for a given number of analog measurements, n_a , taking the maximum number of quantized measurements, n_q , under the power constraint is optimal in terms of minimizing the MSE, as in the optimization problem

given in (27). We show that for any given value of n_a , we obtain that

$$MSE|_{n_a, n_q} - MSE|_{n_a, n_q+1} \geq 0, \quad (79)$$

meaning that the addition of a quantized measurement can only improve the MSE. Substituting the MSE in (18) into (79), we obtain that

$$\begin{aligned} &MSE|_{n_a, n_q} - MSE|_{n_a, n_q+1} \\ &= M - M \left(\frac{\rho_a n_a}{\rho_a n_a + \sigma_a^2} \right. \\ &\quad \left. + \frac{2\rho_q n_q \sigma_a^4}{\pi(\rho_q + \sigma_q^2)(\alpha + \beta(n_a) \rho_q n_q)(\rho_a n_a + \sigma_a^2)^2} \right) \\ &\quad - \left[M - M \left(\frac{\rho_a n_a}{\rho_a n_a + \sigma_a^2} \right. \right. \\ &\quad \left. \left. + \frac{2\rho_q (n_q + 1) \sigma_a^4}{\pi(\rho_q + \sigma_q^2)(\alpha + \beta(n_a) \rho_q (n_q + 1))(\rho_a n_a + \sigma_a^2)^2} \right) \right] \\ &= M \frac{2\rho_q \sigma_a^4}{\pi(\rho_q + \sigma_q^2)(\rho_a n_a + \sigma_a^2)^2} \left[\frac{n_q + 1}{\alpha + \beta(n_a) \rho_q (n_q + 1)} \right. \\ &\quad \left. - \frac{n_q}{\alpha + \beta(n_a) \rho_q n_q} \right] \\ &= M \frac{2\rho_q \sigma_a^4}{\pi(\rho_q + \sigma_q^2)(\rho_a n_a + \sigma_a^2)^2} \\ &\quad \cdot \frac{1}{(\alpha + \beta(n_a) \rho_q (n_q + 1))(\alpha + \beta(n_a) \rho_q n_q)} \geq 0. \end{aligned} \quad (80)$$

In the following, we show that $\beta(n_a) > 0$. First, it can be seen that according to the definition of β in (20) we have

$$\begin{aligned} \beta(n_a) &= \frac{2}{\pi \rho_q} \arcsin \left(\frac{\rho_q}{\rho_q + \sigma_q^2} \right) - \frac{2}{\pi \rho_q} \frac{\rho_a n_a}{\rho_a n_a + \sigma_a^2} \frac{\rho_q}{\rho_q + \sigma_q^2} \\ &= \frac{2}{\pi \rho_q} \left(\arcsin \left(\frac{\rho_q}{\rho_q + \sigma_q^2} \right) - \frac{\rho_a n_a}{\rho_a n_a + \sigma_a^2} \frac{\rho_q}{\rho_q + \sigma_q^2} \right), \end{aligned} \quad (81)$$

where

$$0 \leq \frac{\rho_a n_a}{\rho_a n_a + \sigma_a^2} \leq 1, \quad (82)$$

and since $\rho_a > 0$, $\sigma_a^2 \geq 0$, and $n_a \geq 0$. In addition,

$$0 < \frac{\rho_q}{\rho_q + \sigma_q^2} \leq 1, \quad (83)$$

since $\rho_q > 0$ and $\sigma_q^2 \geq 0$. Therefore, due to (82) and (83), the following expression is also positive

$$\arcsin \left(\frac{\rho_q}{\rho_q + \sigma_q^2} \right) - \frac{\rho_a n_a}{\rho_a n_a + \sigma_a^2} \frac{\rho_q}{\rho_q + \sigma_q^2} > 0, \quad (84)$$

and thus, we can conclude that $\beta(n_a) > 0$. Moreover, as a result of (83), we also have that

$$0 \leq \alpha < 1. \quad (85)$$

Since n_a , n_q , ρ_a , ρ_q , σ_a^2 , σ_q^2 , α , and $\beta(n_a)$ in (80) are non-negative, the inequality in (79) holds. Therefore, given the number of analog measurements, we take the maximum number of quantized measurements possible under the power constraint. This in turn allows us to solve using a one-dimensional search over n_a with the value of n_q given in (29).

REFERENCES

- [1] A. Ribeiro and G. B. Giannakis, "Bandwidth-constrained distributed estimation for wireless sensor networks-part I: Gaussian case," *IEEE Trans. Signal Processing*, vol. 54, no. 3, pp. 1131–1143, Mar. 2006.
- [2] —, "Bandwidth-constrained distributed estimation for wireless sensor networks-part II: unknown probability density function," *IEEE Trans. Signal Processing*, vol. 54, no. 7, pp. 2784–2796, July 2006.
- [3] P. Chavali and A. Nehorai, "Managing multi-modal sensor networks using price theory," *IEEE Trans. Signal Processing*, vol. 60, no. 9, pp. 4874–4887, 2012.
- [4] D. Saska, R. S. Blum, and L. Kaplan, "Fusion of quantized and unquantized sensor data for estimation," *IEEE Signal Processing Letters*, vol. 22, no. 11, pp. 1927–1930, Nov. 2015.
- [5] D. Mandic, M. Golz, A. Kuh, D. Obradovic, and T. Tanaka, *Signal processing techniques for knowledge extraction and information fusion*. US: Springer, 2008.
- [6] R. M. Corey and A. C. Singer, "Wideband source localization using one-bit quantized arrays," in *2017 IEEE 7th International Workshop on Computational Advances in Multi-Sensor Adaptive Processing (CAMSAP)*. IEEE, 2017, pp. 1–5.
- [7] A. Ribeiro, I. D. Schizas, S. I. Roumeliotis, and G. Giannakis, "Kalman filtering in wireless sensor networks," *IEEE Control Systems Magazine*, vol. 30, no. 2, pp. 66–86, Apr. 2010.
- [8] M. Stein, A. Kürzl, A. Mezghani, and J. A. Nossek, "Asymptotic parameter tracking performance with measurement data of 1-bit resolution," *IEEE Trans. Signal Processing*, vol. 63, no. 22, pp. 6086–6095, Nov 2015.
- [9] P. M. Djurić, M. Vemula, and M. F. Bugallo, "Target tracking by particle filtering in binary sensor networks," *IEEE Trans. Signal Processing*, vol. 56, no. 6, pp. 2229–2238, June 2008.
- [10] Y. Li, C. Tao, G. Seco-Granados, A. Mezghani, A. L. Swindlehurst, and L. Liu, "Channel estimation and performance analysis of one-bit massive MIMO systems," *IEEE Trans. Signal Processing*, vol. 65, no. 15, pp. 4075–4089, 2017.
- [11] J. Park, S. Park, A. Yazdan, and R. W. Heath, "Optimization of mixed-ADC multi-antenna systems for cloud-RAN deployments," *IEEE Trans. Communications*, vol. 65, no. 9, pp. 3962–3975, 2017.
- [12] T.-C. Zhang, C.-K. Wen, S. Jin, and T. Jiang, "Mixed-ADC massive MIMO detectors: Performance analysis and design optimization," *IEEE Trans. Wireless Communications*, vol. 15, no. 11, pp. 7738–7752, 2016.
- [13] N. Liang and W. Zhang, "Mixed-ADC massive MIMO," *IEEE Journal on Selected Areas in Communications*, vol. 34, no. 4, pp. 983–997, 2016.
- [14] J. Choi, J. Mo, and R. W. Heath, "Near maximum-likelihood detector and channel estimator for uplink multiuser massive MIMO systems with one-bit ADCs," *IEEE Trans. Communications*, vol. 64, no. 5, pp. 2005–2018, May 2016.
- [15] H. Pirzadeh and A. L. Swindlehurst, "Spectral efficiency of mixed-ADC massive MIMO," *IEEE Trans. Signal Processing*, vol. 66, no. 13, pp. 3599–3613, 2018.
- [16] N. Shlezinger, Y. C. Eldar, and M. R. Rodrigues, "Asymptotic task-based quantization with application to massive MIMO," *IEEE Trans. Signal Processing*, vol. 67, no. 15, pp. 3995–4012, 2019.
- [17] T. L. Marzetta, "Noncooperative cellular wireless with unlimited numbers of base station antennas," *IEEE trans. wireless communications*, vol. 9, no. 11, pp. 3590–3600, 2010.
- [18] J. Lunden, V. Koivunen, and H. V. Poor, "Spectrum exploration and exploitation for cognitive radio: Recent advances," *IEEE Signal Processing Magazine*, vol. 32, no. 3, pp. 123–140, May 2015.
- [19] O. Bar-Shalom and A. J. Weiss, "DOA estimation using one-bit quantized measurements," *IEEE Trans. Aerospace and Electronic Systems*, vol. 38, no. 3, pp. 868–884, 2002.
- [20] R. H. Walden, "Analog-to-digital converter survey and analysis," *IEEE Journal on selected areas in communications*, vol. 17, no. 4, pp. 539–550, 1999.
- [21] Bin Le, T. W. Rondeau, J. H. Reed, and C. W. Bostian, "Analog-to-digital converters," *IEEE Signal Processing Magazine*, vol. 22, no. 6, pp. 69–77, Nov 2005.
- [22] H. C. Papadopoulos, G. W. Wornell, and A. V. Oppenheim, "Sequential signal encoding from noisy measurements using quantizers with dynamic bias control," *IEEE Trans. Information Theory*, vol. 47, no. 3, pp. 978–1002, Mar. 2001.
- [23] M. S. Stein, S. Bar, J. A. Nossek, and J. Tabrikian, "Performance analysis for channel estimation with 1-bit ADC and unknown quantization threshold," *IEEE Trans. Signal Processing*, vol. 66, no. 10, pp. 2557–2571, May 2018.
- [24] A. Host-Madsen and P. Handel, "Effects of sampling and quantization on single-tone frequency estimation," *IEEE Trans. Signal Processing*, vol. 48, no. 3, pp. 650–662, Mar. 2000.
- [25] A. Kipnis and J. C. Duchi, "Mean estimation from one-bit measurements," *CoRR*, vol. abs/1901.03403, 2019. [Online]. Available: <http://arxiv.org/abs/1901.03403>
- [26] G. Wang, J. Zhu, R. S. Blum, P. Willett, S. Marano, V. Matta, and P. Braca, "Signal amplitude estimation and detection from unlabeled binary quantized samples," *IEEE Trans. Signal Processing*, vol. 66, no. 16, pp. 4291–4303, Aug. 2018.
- [27] M. S. Stein, "Spectral power parameter estimation of random sources with binary sampled signals," 2019.
- [28] J. Zhu, X. Lin, R. S. Blum, and Y. Gu, "Parameter estimation from quantized observations in multiplicative noise environments," *IEEE Trans. Signal Processing*, vol. 63, no. 15, pp. 4037–4050, Aug. 2015.
- [29] J. Ren, T. Zhang, J. Li, and P. Stoica, "Sinusoidal parameter estimation from signed measurements via majorization-minimization based RELAX," *IEEE Trans. Signal Processing*, vol. 67, no. 8, pp. 2173–2186, Apr. 2019.
- [30] G. Zeitler, G. Kramer, and A. C. Singer, "Bayesian parameter estimation using single-bit dithered quantization," *IEEE Transactions on Signal Processing*, vol. 60, no. 6, pp. 2713–2726, 2012.
- [31] S. Jacobsson, G. Durisi, M. Coldrey, U. Gustavsson, and C. Studer, "One-bit massive MIMO: Channel estimation and high-order modulations," in *IEEE International Conference on Communication Workshop (ICCW)*, 2015, pp. 1304–1309.
- [32] Q. Wan, J. Fang, H. Duan, Z. Chen, and H. Li, "Generalized Bussgang LMMSE channel estimation for one-bit massive MIMO systems," *IEEE Transactions on Wireless Communications*, 2020.
- [33] N. Harel and T. Routtenberg, "Non-Bayesian estimation with partially quantized observations," in *International Conference on Digital Signal Processing (DSP)*, 2017, pp. 1–5.
- [34] F. Gustafsson and R. Karlsson, "Generating dithering noise for maximum likelihood estimation from quantized data," *Automatica*, vol. 49, no. 2, pp. 554–560, 2013.
- [35] O. Dabeer and E. Masry, "Multivariate signal parameter estimation under dependent noise from 1-bit dithered quantized data," *IEEE Trans. Information Theory*, vol. 54, no. 4, pp. 1637–1654, 2008.
- [36] S. Boyd and L. Vandenberghe, *Convex Optimization*. Cambridge University Press, 2004.
- [37] E. Vlachos and J. Thompson, "Dithered beamforming for channel estimation in mmwave-based massive MIMO," in *2018 IEEE International Conference on Acoustics, Speech and Signal Processing (ICASSP)*. IEEE, 2018, pp. 3604–3608.
- [38] L. Lu, G. Y. Li, A. L. Swindlehurst, A. Ashikhmin, and R. Zhang, "An overview of massive MIMO: Benefits and challenges," *IEEE journal of selected topics in signal processing*, vol. 8, no. 5, pp. 742–758, 2014.
- [39] H. Pirzadeh and A. L. Swindlehurst, "Spectral efficiency under energy constraint for mixed-ADC MRC massive MIMO," *IEEE Signal Processing Letters*, vol. 24, no. 12, pp. 1847–1851, 2017.
- [40] S. Jacobsson, G. Durisi, M. Coldrey, U. Gustavsson, and C. Studer, "Throughput analysis of massive MIMO uplink with low-resolution ADCs," *IEEE Trans. Wireless Communications*, vol. 16, no. 6, pp. 4038–4051, 2017.
- [41] E. G. Larsson, O. Edfors, F. Tufvesson, and T. L. Marzetta, "Massive MIMO for next generation wireless systems," *IEEE communications magazine*, vol. 52, no. 2, pp. 186–195, 2014.
- [42] A. Puglielli, A. Townley, G. LaCaille, V. Milovanović, P. Lu, K. Trotskovsky, A. Whitcombe, N. Narevsky, G. Wright, T. Courtade *et al.*, "Design of energy-and cost-efficient massive mimo arrays," *Proceedings of the IEEE*, vol. 104, no. 3, pp. 586–606, 2015.
- [43] A. Papoulis, *Probability, random variables and stochastic processes*, 4th ed. Boston: McGraw-Hill, 2002.
- [44] J. J. Bussgang, "Crosscorrelation functions of amplitude-distorted gaussian signals," *Research Laboratory of Electronics, Massachusetts Institute of Technology*, 1952.
- [45] R. A. Horn and C. R. Johnson, *Matrix analysis*. Cambridge university press, 2012.

This figure "SystemSchemeV2.jpg" is available in "jpg" format from:

<http://arxiv.org/ps/2009.08081v1>